

SUPPLEMENTARY MATERIAL

A) LASER DISPERSION ANALOGUE EXPERIMENTS

To infer the composition of organic-bearing ice grains, we have used analogue experiments in Heidelberg to reproduce CDA in situ “organic-bearing” mass spectra. The laboratory setup is able to simulate the impact ionization process and recreate the mass spectra of ice particles impinging onto impact ionization spectrometers like the Cassini Cosmic Dust Analyzer, CDA (Postberg et al. 2009a; Klenner et al. 2019). With the analogue experiment a micron-sized water beam with dissolved substances (i.e. organic or inorganic compounds) is exposed to an adjustable pulsed infrared laser. The combination of varying laser intensity on the liquid beam and delay time settings for ion extraction (Charvat et al. 2004) simulates a variety of impact energies of ice grains at hypervelocities onto the CDA target (Klenner et al. 2019). This experimental procedure thus generates cations, anions and the neutral species of water and dissolved substances that are similar to those species produced by impact ionization of ice grains with CDA (Fig. SM 1) (Postberg et al. 2009a; Wiederschein et al. 2015).

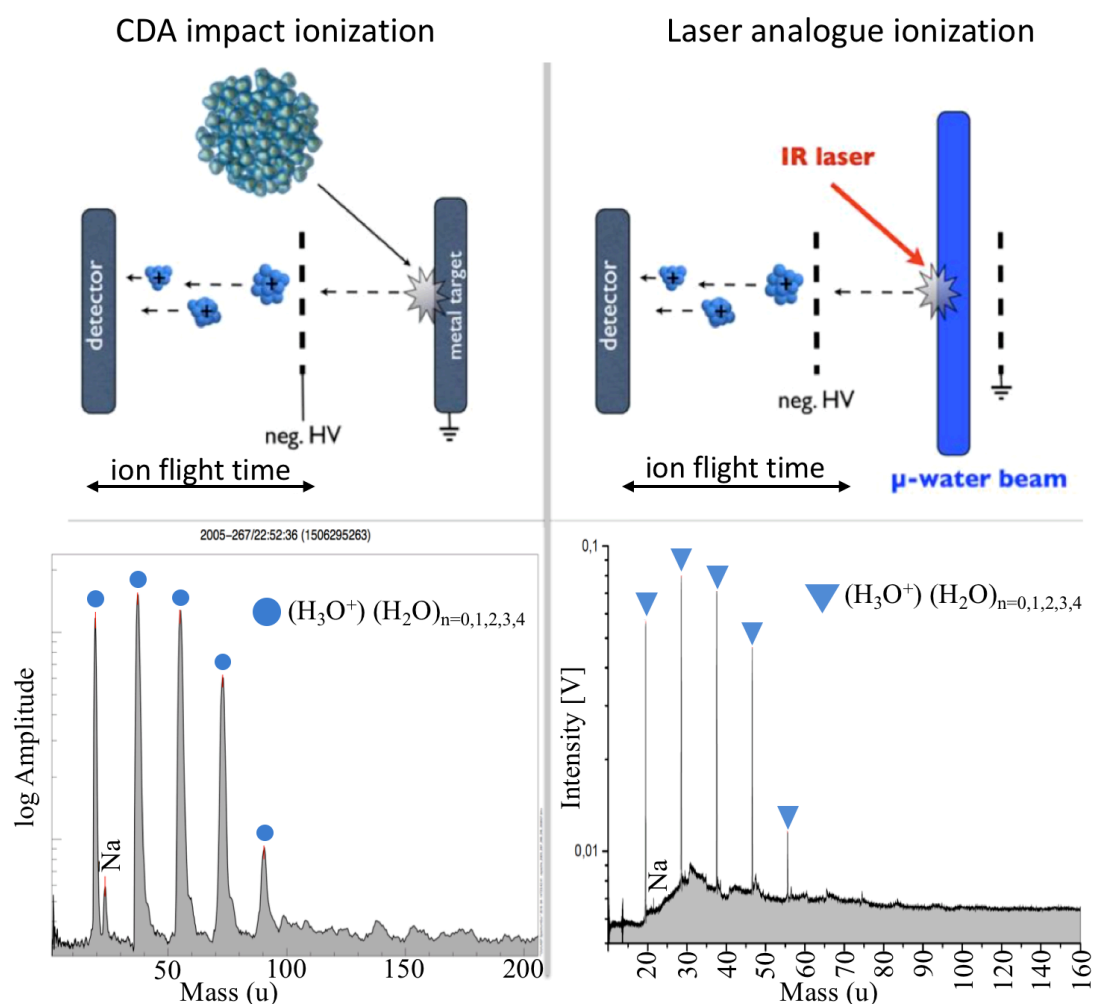


Figure SM 1. Comparison of the ionization mechanisms used by CDA and in the laboratory. (Top) Schematics of the CDA impact ionization process of a high velocity impact of a micron-sized ice grain (left) and the analogue process by laser dispersion of a water beam in the laboratory (right). The analogue experiment ionizes analyte from the liquid phase, in contrast to CDA where it is ionized from the solid phase.

However, both processes produce similar cationic fragment clusters. (Bottom) The CDA in situ spectrum of an almost pure water ice grain (left) and the laser-produced spectrum of a pure liquid water beam (right) is shown. These spectra show that the laser-assisted analogue experiment accurately reproduces CDA mass spectra. Adapted from Postberg et al. 2009a.

The laser-assisted analogue experiment has been proven to be a valid analogue setup for reproducing the characteristic peak patterns of Type 1 (Fig. SM 1) and Type 3 (Postberg et al. 2009a) E ring ice grains. The consistent spectral features of these ice grains are easily reproduced in the laboratory. In contrast, organic-enriched (Type 2) ice grains display a great diversity in peak patterns, indicating varying contributions from multiple organic compounds. However, we are also able to reproduce some of the cationic fragments observed in CDA Type 2 spectra (Postberg et al. 2018a; Klenner et al. 2019), which can be attributed to characteristic fragments of different classes of organic compounds.

To identify the fragments observed in CDA Type 2 spectra, and to infer the composition of organic material, we have measured water-dissolved organic compounds (Sigma-Aldrich, purity ≥ 95.0 per cent (see Supplementary Material (SM) Tables SM 1, 2, 3).

B) CDA DATA ANALYSIS: DATA REDUCTIONS AND SELECTION CRITERIA

The CDA was designed to determine the speeds, masses, electric charges and compositions of micron- and sub-micron dust particles in the Saturnian system (Srama et al. 2004). The Chemical Analyzer (CA) subsystem of the CDA is responsible for the chemical characterization of an impacting dust particle (Srama et al. 2004). Depending on their trajectories, dust particles hit either the CDA's central rhodium target plate (chemical analyzer target; CAT) or the surrounding gold target (or the inner walls of the instrument). This work considers dust impacts onto the CAT only, for which compositional information can then be derived. The CAT is held at $\sim +1000$ V with respect to an electrically-grounded grid approximately 3 mm in front of it. When a dust particle hits the CAT at high velocity ($\geq 1\text{-}3$ km s⁻¹) it is partly ionized (the degree of ionization increases with impact speed). The impact thus creates a plasma cloud, consisting of ions from the particle and the target along with electrons and neutral molecules and atoms. The positively-charged target collects electrons and negative ions (anions) from the plasma cloud and accelerates positive ions (cations) towards an ion detector and amplifier, the multiplier, through a near field-free region approximately 20 cm long. The spectrometer is sensitive to cations only and generates cationic Time of Flight (TOF) mass spectra. The mass resolution of these spectra, $m/\Delta m$, varies between 10-50 depending on the atomic masses of ions \sim from 1 u to 190 u. Spectrum recording may be triggered by impacts when the negative charge collected at the CAT exceeds a preset threshold, or when the positive charge of the first abundant cationic species exceeds a threshold at the multiplier. In the latter case, the recording can be triggered up to several microseconds after the impact of a particle onto the CAT. For water-dominated ice particles frequently abundant species are H⁺ or H₃O⁺. In the case of spectrum recording triggered by the arrival of abundant hydronium ions (H₃O⁺), mass lines corresponding to species having masses lower than 19 u, including H₃O⁺ itself, are

not visible in the spectrum. For a detailed description of the CDA and its subsystems, see Srama et al. (2004).

In this study we considered 731 Type 2 spectra recorded from November 2004 until May 2008 in the E ring. Only those spectra that included mass lines between 26 u — 31 u (low mass organic signature (LMOS)) and/or between 39 u — 45 u with amplitudes of at least 2.5-sigma significance above the noise amplitude were considered. These spectra were triggered directly by impact or by registering an abundant ion species (mass < ~ 18 u) at the multiplier. During Cassini's E5 flyby of Enceladus (Postberg et al. 2011) in October 2008, the instrument became insensitive to triggering spectrum recording by particle impact. Thus, after this period most of the CDA spectra were triggered by registering H₂O⁺ or Na⁺ ions at the multiplier, whereas spectrum recording triggered by particle impact was rarely observed. The multiplier-triggered spectra for which recording was triggered by ions with masses greater than 17 u do not fulfil our selection criteria and were not taken into account for this study. Datasets collected before the E5 flyby also show negligible instrument contamination from salt accumulated on the CAT during deep Enceladus plume dives from 2004 to 2008, unlike later datasets.

The methodology used to calibrate the datasets (apply a mass scale) was described in Postberg et al. (2006, 2008) and performed here using water and sodium mass lines. The following are the periods (expressed in seconds), in which Type 2 spectra fulfilled our criteria, as recorded by the spacecraft clock:

- 1477548025 – 1477746968
- 1489004979 – 1489118561
- 1493765055 – 1493767792
- 1495335775 – 1495511751
- 1496912995 – 1496913753
- 1498469760 – 1498505448
- 1503216429 – 1503223309
- 1504603798 – 1504604417
- 1506183784 – 1506226665
- 1509311996 – 1509357627
- 1514090477 – 1514186815
- 1519590629 – 1519613920
- 1526853639 – 1526888436
- 1530413463 – 1530439257
- 1557517652 – 1557520425
- 1558908829 – 1558912626
- 1561672925 – 1561698421
- 1575350272 – 1575350678
- 1589065736 – 1589083623

A large number of organic-bearing spectra (Type 2) show non-water spectral features in addition to the LMOS. In this study we have identified three such different features in a relatively large number of Type 2 spectra. We applied stringent criteria to identify spectra (60 archetype spectra) that clearly show at least one of these specific features.

We have attributed these spectral features to fragment cations characteristic to N-bearing, O-bearing or Aromatic organic compounds. As a consequence of our conservative selection criteria, a large number of spectra possessing these specific features, but at comparatively low amplitudes (significance), were not included in the study. Therefore, the number of Type 2 spectra categorized into the sub-groups discussed here represents the lower bound of our data. The selection criteria used to assign each spectrum to a specific organic class are:

B1) N-bearing spectra

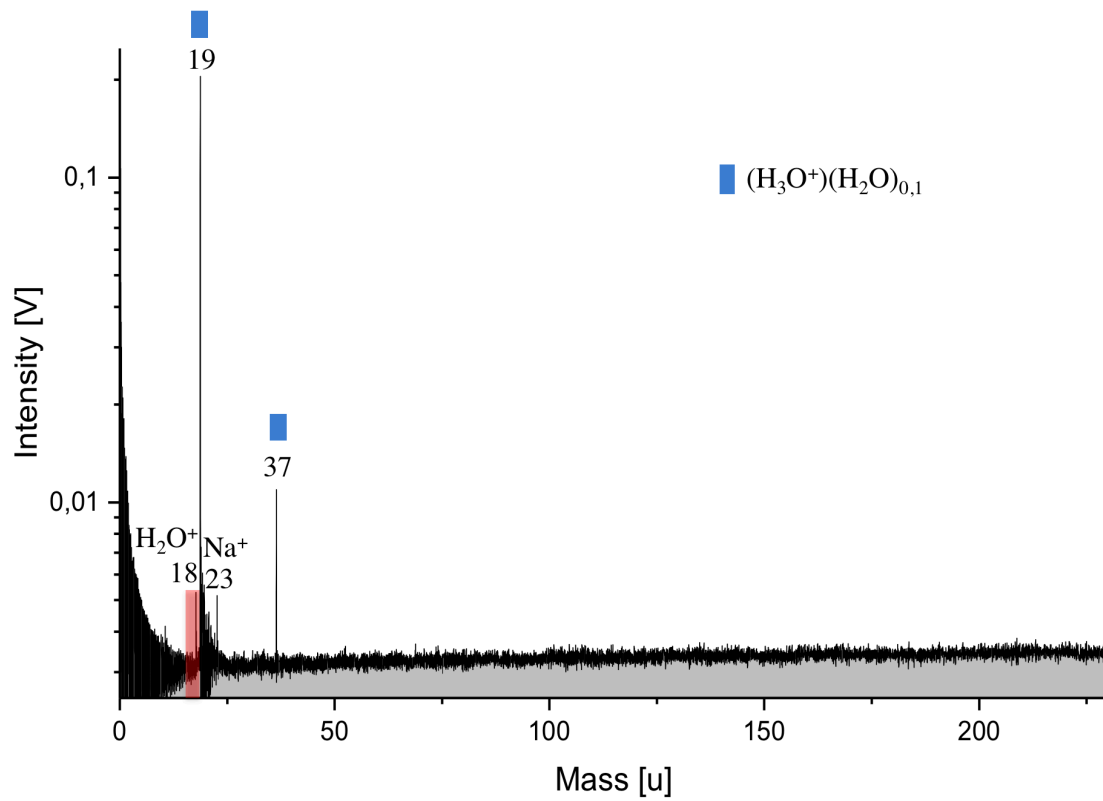
The spectra are considered as N-bearing if they show a mass line at 18 u, which we attribute to ammonium cations (NH_4^+). The amplitude ratio of 18 u/19 u in these spectra must be at least 0.2 and the apparent mass difference (Δm) between these two peaks must be ~ 0.7 u — 1.4 u. In this subgroup we selected only those CDA Type 2 spectra that were triggered by impact. The absence of mass lines corresponding to hydrogen cations (H^+) and the CDA rhodium target plate at 103 u (i.e. Rh^+) implies that these spectra were recorded at low energy densities (Postberg et al. 2009b; Klenner et al. 2019), equivalent to impact speeds below 8.5 km s⁻¹. Calibration of this spectral type was done by using water and sodium mass lines, together with suitable stretch parameters (Hillier et al. 2007; Postberg et al. 2009b)

In principle NH_4^+ could be produced from ammonia gas adsorbed onto the preexisting ice grains in the icy vents. However, this scenario is highly unlikely, for multiple reasons: Firstly, He, Acharyya & Vidali (2016) investigated the binding energy of ammonia onto crystalline water ice. They deposited ammonia at 50 K and found that, with increasing temperature, the desorption of ammonia started immediately and it was completely desorbed by 145 K. Therefore, ammonia is unlikely to be, or remain, adsorbed onto ice grains within the Enceladean ice vents where the temperature range is expected between 272-190 K, and almost certainly above 145 K (Postberg et al. 2018a). The maximum possible, surface coverage dependent, binding energy was found to be 4000 K (~ 0.3 eV), much lower than that required for adsorption onto ice grains as described by Bouquet et al. 2019.

Secondly, the adsorption of ammonia, if possible despite the binding energy argument above, must occur on all types of ice grains, given the abundance of NH_3 in the plume. However, unambiguous peaks at 18 u, over the velocity range described here, only correlate with organic features and do not appear in spectra of Type 1 and Type 3 grains. This further makes it highly unlikely that ammonia is a source of NH_4^+ in the N-bearing Type 2 spectra.

One has to consider also the possibility of H_2O^+ interfering with ammonium cations at 18 u. In order to estimate how much H_2O^+ could be generated from water particle impacts, we measured pure water at varying laser intensities and delay time settings in the analogue laboratory setup (Klenner et al. 2019). In these spectra we detected H_2O^+ only at high energy densities (Fig. SM 2 top), which correspond to a similar feature observed in CDA near-pure water ice spectra (Type I) at impact speeds much greater than 8 km s⁻¹ (Fig. SM 2 bottom). Additionally, the amplitude ratio of 18 u / 19 u in spectra generated this way is ≤ 0.1 , much lower than in CDA N-bearing spectra (Fig. 2). To exclude significant contributions of H_2O^+ we excluded all spectra showing a clear Rh^+ mass line, the generation of which requires a minimum speed of ~ 8 km s⁻¹ (Postberg

et al. 2009b). To maintain a very conservative selection we furthermore only considered spectra with an unusually high amplitude ratio of $18 \text{ u} / 19 \text{ u} \geq 0.2$ (Fig. 2). Therefore, the peak observed in CDA N-bearing spectra is, at least to a greater part, if not exclusively, from NH_4^+ and not H_2O^+ .



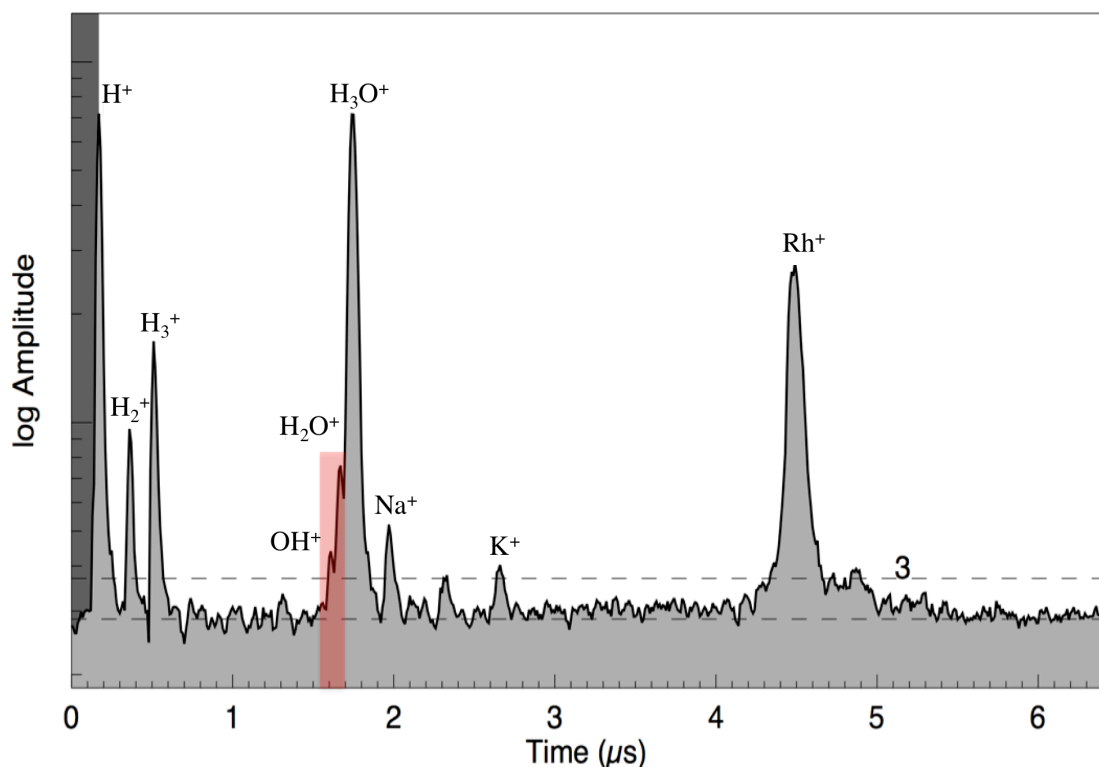


Figure SM 2. Comparison of laboratory and CDA spectra (Top) A laboratory spectrum of pure water at high laser energy density shows a minor peak at 18 u, which is attributed to H_2O^+ (marked in red). Water-cluster species are marked blue. (Bottom) A CDA spectrum of an ice grain impacting at a speed of 14.5 km s^{-1} shows a minor H_2O^+ peak (marked in red) at 18 u, similar to that in the laboratory spectrum (top).

B2) O-bearing spectra

The positive identification of O-bearing species only occurred when a peak at 43 u or at 45 u was higher than any adjacent peaks in the 41 u to 45 u range. This means the $43 \pm 0.5 \text{ u}$ or the $45 \pm 0.5 \text{ u}$ signature had to be clearly separated from the abundant water cluster peak at 37 u. This is a very restrictive criterion as it excludes spectra that either showed abundant C_3 hydrocarbon fragments (see below) interfering in this mass region, or spectra with an abundant sodium-water cluster at 41 u ($\text{Na-H}_2\text{O}^+$). In both cases $\text{C}_2\text{H}_3\text{O}^+$ or $\text{C}_2\text{H}_5\text{O}^+$ ions (at 43 or 45 u respectively) would then be accompanied by mass lines, near the neighbouring large water cluster peak at 37 u, that would prevent the formation of an isolated peak at 43 u or 45 u.

In principle a mass line at 43 u can be produced by O-bearing species (e.g., carbonyls/hydroxyls) as $\text{C}_2\text{H}_3\text{O}^+$ and/or hydrocarbons (C_3H_7^+). However, stoichiometry means that, for N-free compounds, the mass line at 45 u can only be produced by O-bearing compounds such as $\text{C}_2\text{H}_5\text{O}^+$. The following arguments also strongly favor O-bearing compounds as the main source of the 43 u peak in the selected spectra, although we cannot completely rule out the contribution of hydrocarbons to this particular mass line.

- Generally, hydrocarbons with $\text{C} \geq 3$ produce a pair of propyl cations at 41 u and 43 u (C_3H_7^+) jointly with a pair of cations at lower masses 27 u and 29 u

($C_2H_{3.5}^+$) (Srama et al. 2009; Le Roy et al. 2015; McLafferty & Turecek 1993; Terrence A. Lee 1998). Depending on the type of hydrocarbons (e.g. saturated or unsaturated) the relative peak intensities of carbocations at C2 and C3 varies. In O-bearing CDA spectra a mass line at 41 u is by definition lower than 43 u, which would indicate the presence of saturated hydrocarbons, in which alkyl cations ($C_3H_7^+$) tend to have the highest intensity. However, in this case the peak intensities of alkyl cations (43 u and 29 u) should correlate with each other, which is not observed in CDA O-bearing spectra.

- These spectra show pure water cluster features with broad right flanks, indicating water clusters with polar species at 43 u (Fig. 4). Such water clusters are not observed with hydrocarbons (Postberg et al. 2018a). This implies that the 43 u feature is potentially O-bearing.
- In some of these spectra the LMOS feature shows a tendency to peak towards the higher end of its typical mass range (26 u – 31 u), which indicates the presence of polar, possibly O-bearing species, in agreement with formyl cations (CH_2O^+ , 30 u, 31 u) (Fig. 4). Alternative interpretations of the 30-31 u signatures as water-carbon clusters ($C^+(H_2O)$ and CH_3O^+ respectively) were given by Hillier et al. (2007) and Postberg et al. 2009b. However, the 31u feature does not appear at low velocities in all spectra, as would be expected if neutral carbon-water clusters, formed from surface contamination (e.g. Postberg et al. 2009b), are protonated in the impact plasma, forming CH_3O^+ . Formation of the 30 u, $C^+(H_2O)$, feature requires impact velocities higher (10 km s⁻¹, Postberg et al. 2009b) than those which created the O-bearing spectra discussed here (< ~ 8.5 km s⁻¹). Therefore, we rule out the possibility of carbon-water clustering (Postberg et al. 2009b) at these masses (30 u, 31 u).
- The pattern of the amplitudes of pure water clusters (spectral envelope) in most of the O-bearing spectra with the 43 u peak is similar to that of spectra with a distinct/isolated peak at 45 u that represents O-bearing cations. This indicates that similar organic species are responsible for this kind of spectral appearance and hence indicating O-bearing species.
- We clearly identify McLafferty re-arrangement, characteristic mainly for carbonyl compounds, in one CDA O-bearing spectrum with a distinct and isolated peak at 43 u and have reproduced it in the laboratory (Fig. SM 3). In addition, a substantial fraction of O-bearing CDA spectra hint at the occurrence of the McLafferty mechanism. From this mechanism we infer (see caption Fig. SM 3) the number of carbon atoms as four in the parent molecules of these O-bearing species.

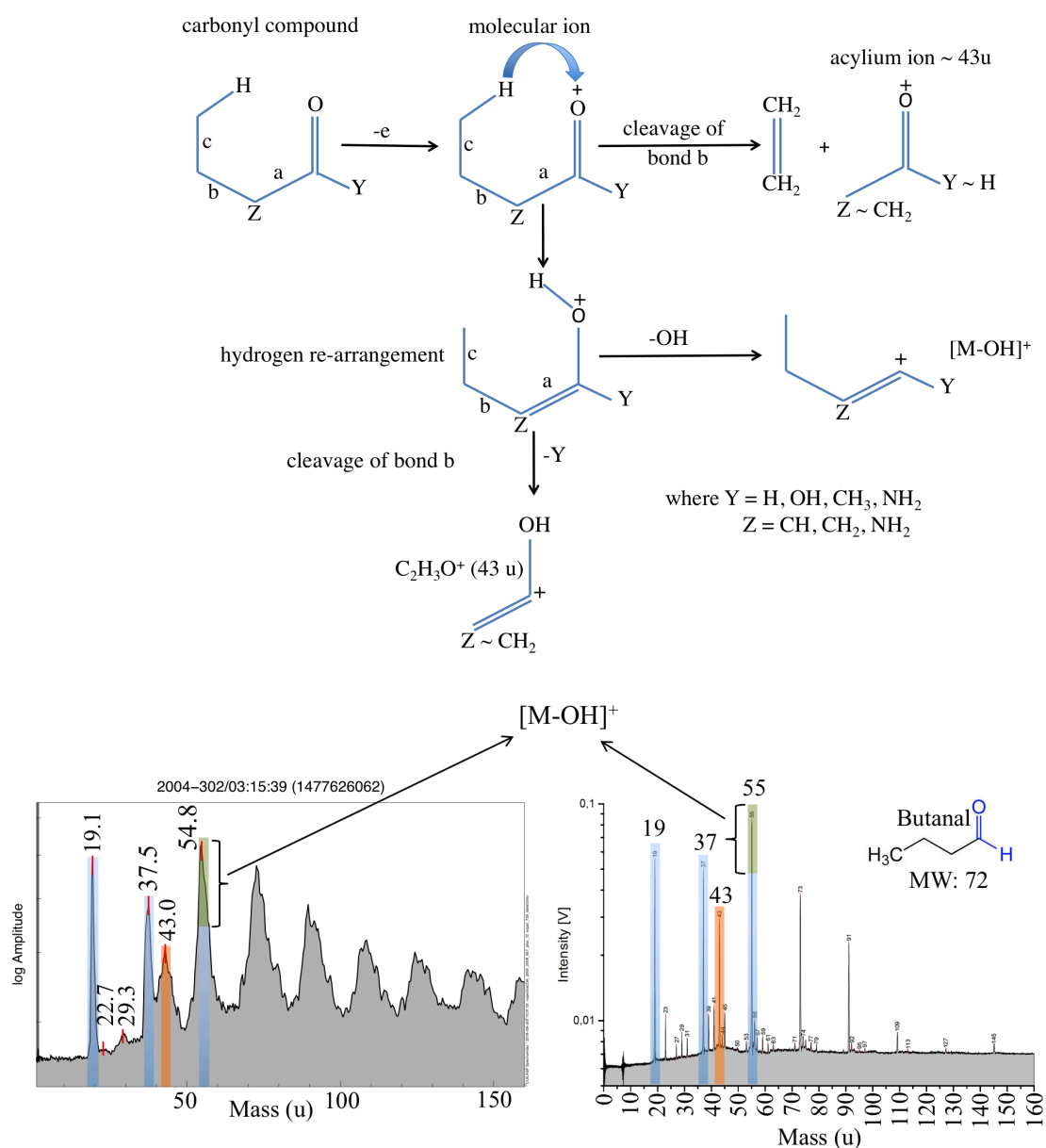


Figure SM 3. McLafferty rearrangement mechanism. Carbonyl compounds can transfer a hydrogen from the gamma-carbon to its double-bonded oxygen. This mechanism is applicable only in carbonyl compounds which contain at least four carbon atoms. During this process, an electron is eliminated from the oxygen atom forming a molecular cation. Subsequently the alkene is eliminated leading to the formation of an acylium cation $[C_2H_3O]^+$. During this re-arrangement of a carbonyl molecule a fragment cation $[M-OH]^+$ is also formed. (Bottom) A CDA O-bearing spectrum (left) is shown. Marked in orange is the characteristic cationic fragment of carbonyl compounds (acylium) and water-clusters are marked in blue. The increase in the peak amplitude at 55 u, marked green, indicates a contribution from non-water cations in addition to water-cluster species. We propose the McLafferty rearrangement mechanism is also responsible for this increase, which we reproduce in the laboratory spectrum (right) of butanal at a concentration of 0.15 mol L⁻¹. As in the CDA spectrum, in the case of butanal, the peak at 55 u is increased by the presence of $[M-OH]^+$. Furthermore, the loss of OH during this mechanism can be confirmed by a C₁₃ isotopic peak of $[M-OH]^+$.

at 56 u present in the lab spectrum, indicating a contribution of non-water species at 55 u.

B3) Aromatic-type spectra

The impinging of almost pure water ice particles onto the instrument target produces the majority of the CDA impact spectra. The water and water-cluster ($\text{H}_3\text{O}^+(\text{H}_2\text{O})_{n=0,1,2,3,\dots}$) peaks dominate in most of the CDA water ice spectra (i.e., Type 1 & Type 2) (Postberg et al. 2008). Often these also exhibit Na-water clusters i.e., $\text{Na}^+(\text{H}_2\text{O})_{n=1,2,3}$ (Postberg et al. 2008) and possibly also K-water clusters i.e., $\text{K}^+(\text{H}_2\text{O})_{n=1,2,3}$.

In many Type 2 spectra these clusters coincide with peaks due to fragment cations of organic compounds and obscure their identification in the ice grains. In the case of CDA aromatic type spectra we have found a peak at m/z 77, which is attributed to phenyl cations and can be used to verify the existence of aromatic compounds in ice grains. However, in most Type 2 spectra, the Na-water cluster $\text{Na}^+(\text{H}_2\text{O})_3$ and possibly the K-water cluster $\text{K}^+(\text{H}_2\text{O})_2$, at 77 u and 75 u respectively, can overlap with phenyl cations (C_6H_5^+) and the limited instrument resolution does not allow classification of those spectra as aromatic type. Only in a very few instances (exemplary archetypal Type 2 spectra, Table SM 4), we are able to distinguish phenyl cations (77 u) from Na- and K-water clusters. In most of these spectra the amplitudes of Na-water clusters, if present, appear as an exponential envelope, in which the peak at 41 u has the highest amplitude. The subsequent clusters at 59 u and 77 u should follow the systematic decrease in their amplitudes. However, we have often observed a sharp increase in the amplitude of the mass line at 77-79 u, which indicates the existence of more than one species at the same mass line e.g. phenyl cations (Fig. 6). In this way, the 77 u peak, together with other coincident aromatic fragment cations confirms the existence of aromatic compounds in the ice grains. In a very few instances the peak at 77 u tends to appear at around 76 u, possibly representing dehydrophenyl cations (C_6H_4^+).

Fragmentation pattern of aromatic compounds in the analogue experiment

Amongst several aromatic compounds (Table SM 3) tested in the analogue experiment, only monocyclic aromatic compounds (MAC) resulted in the formation of the observed aromatic cationic fragment series. As an example of typical mass spectral features arising from phenyl-group compounds, the laboratory spectrum of aniline (Fig. SM 4 top) shows a strong peak at 77 u from C_6H_5^+ in good agreement with CDA spectra. The loss of neutral acetylene (C_2H_2) from 77 u produces C_4H_3^+ at 51 u (Fig. SM 6). However, the peak corresponding to tropylium cations is not observed as it forms when there is a benzyl group present. For example, benzyl amine shows a dominant tropylium peak at 91 u (C_7H_7^+) (Fig. SM 4 bottom). Here, the loss of acetylene (C_2H_2) from the tropylium cation produces C_5H_5^+ at 65 u, which further loses acetylene to form C_3H_3^+ at 39 u (Fig. SM 6).

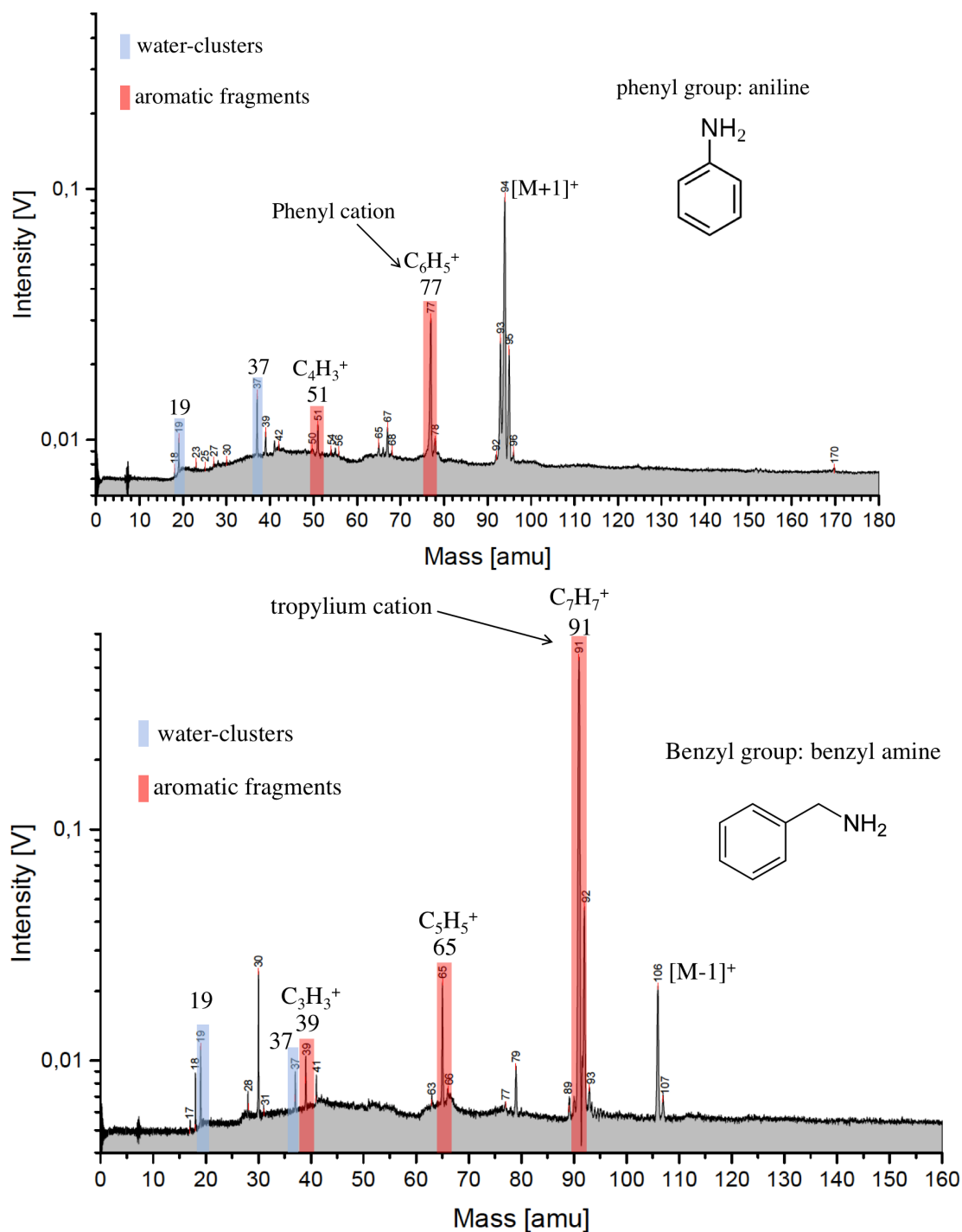


Figure SM 4. Laboratory spectra of the phenyl group compound (aniline, top) and the benzyl group compound (benzyl amine, bottom) measured at concentrations of 0.05 mol L⁻¹ in H₂O. Fragment cations are marked in red. Phenyl group compound (aniline) yields a high abundance of C₆H₅⁺ at 77 u. In contrast, the benzyl group compound (benzyl amine) more efficiently produces C₇H₇⁺ at 91 u. Other aromatic fragment cations described in the text are also visible at 51 u in the aniline spectrum and 65 u & 39 u in the benzyl amine spectrum. The unmarked organic fragments are specific to each compound. As previously, water-clusters are marked in blue.

In order to reproduce in the laboratory, the relative abundance of phenyl and tropylium cations, as found in CDA aromatic-type spectra, we used a mixture of benzoyl and

benzyl group compounds. For example, an aqueous mixture of benzoic acid and phenyl acetaldehyde results in the efficient formation of phenyl cations in parallel with a low level of tropylium (Fig. SM 5), as typically observed in aromatic CDA spectra (Fig. 6). The mass lines at 77 u and 79 u derive from benzoic acid (deprotonated and protonated benzene-derived cations, $C_6H_5^+$ and $C_6H_7^+$), whereas those at 91 u and 93 u are produced from phenyl acetaldehyde ($C_7H_7^+$ & $C_7H_9^+$). The aromatic-related fragment ions at lower masses are also visible (65 u, 67 u, 51 u, 53 u and 39 u). The overall peak pattern from the mixture of these two different groups of aromatic compounds is in good agreement with the peak pattern (Fig. SM 6 & Table SM 3) typically observed in CDA aromatic-type spectra. This mixture is by no means unique in producing such a pattern, but demonstrates that at least two different aromatic configurations are required to explain the observation.

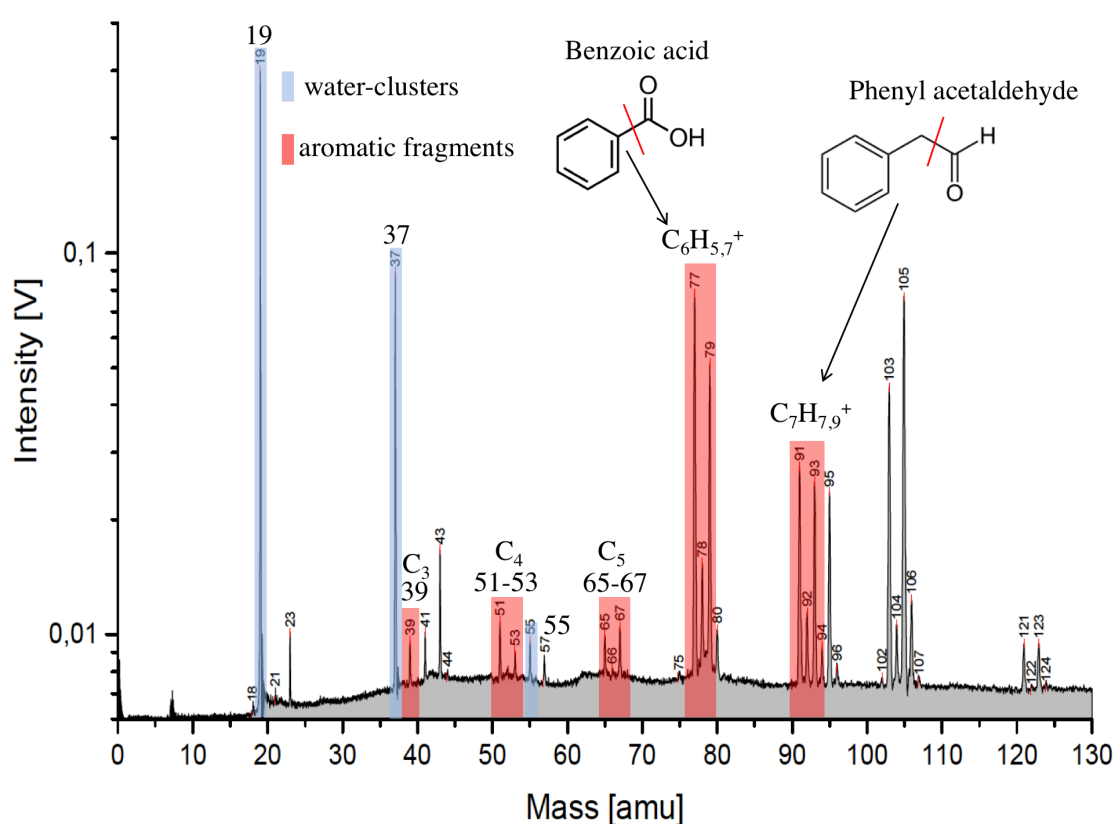


Figure SM 5. Laboratory spectrum from a mixture of benzoyl and benzyl group species – benzoic acid and phenyl acetaldehyde. Spectrum from 0.026 mol L⁻¹ of benzoic acid and 0.015 mol L⁻¹ of phenyl acetaldehyde dissolved in H₂O. Aromatic fragment cations from both organic compounds are highlighted in red. $C_6H_{5,7}^+$ comes from benzoic acid and $C_7H_{7,9}^+$ from phenyl acetaldehyde. The peak pattern of the aromatic fragment cations matches the observed peak pattern in CDA aromatic-type spectra, where $C_6H_{5,7}^+$ is more abundant than $C_7H_{7,9}^+$. Other relevant aromatic fragments corresponding to C₃, C₄, and C₅ with different numbers of hydrogen atoms are also marked red.

C) EXTENDED DATA

In this section we include tables of measured organic compounds (which do not necessarily include all species mentioned in Table SM 6), a figure of fragmentation pathways for aromatic compounds and a list of archetypal CDA spectra. List of re-analysed HMOC data and related figures are also included. Also a figure of the lab spectrum of pyruvic acid is included.

Table SM 1. N-bearing compounds measured in the analogue laboratory experiment. Molecular weights and the characteristic fragment ions in the spectra are listed here. Apart from N-heterocyclic compounds, all other N-bearing compounds produce a high abundance of ammonium cations corresponding to a mass line at 18 u in the laboratory.

Molecule	Formula	Struc. formula	Mol. weight	Mol. peak	Ammon. cation
<i>Alkanolamines</i>					
Ethanolamine	C ₂ H ₇ NO		61	[M+1] ⁺	18
5-Amino-1-pentanol	C ₅ H ₁₃ NO		103	[M+1] ⁺	18
<i>Primary alkylamines</i>					
Ethylamine	C ₂ H ₇ N		45	[M+1] ⁺	18
Butylamine	C ₄ H ₁₁ N		73	[M+1] ⁺	18, 17 (minor)
<i>Aromatic amines</i>					
Benzylamine	C ₇ H ₉ N		107	[M-1] ⁺	18
Aniline	C ₆ H ₇ N		93	[M+1] ⁺	18 (minor)
<i>Primary alkyl nitriles</i>					
Acetonitrile	C ₂ H ₃ N		41	[M+1] ⁺	---
Propionitrile	C ₃ H ₅ N		55	[M+1] ⁺	18
Valeronitrile	C ₅ H ₉ N		83	[M+1] ⁺	18
<i>Aromatic nitriles</i>					
Mandelonitrile	C ₈ H ₇ NO		133	[M-1] ⁺	18
<i>Aromatic nitros</i>					
4-Nitrophenol	C ₆ H ₅ NO ₃		139	[M+1] ⁺	18 (minor)
2-Nitroresorcin	C ₆ H ₅ NO ₄		155	[M+1] ⁺	18
<i>N-heterocyclic</i>					
Nicotinic acid	C ₆ H ₅ NO ₂		123	[M+1] ⁺	---
Pyridine	C ₅ H ₅ N		79	[M+1] ⁺	---
Pyrimidine	C ₄ H ₄ N ₂		80	[M+1] ⁺	18 (minor)
Quinoline	C ₉ H ₇ N		129	[M+1] ⁺	---

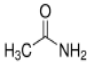
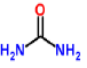
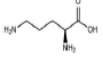
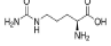
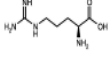
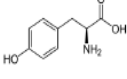
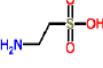
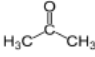
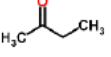
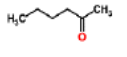
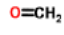
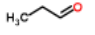
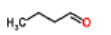

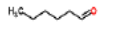
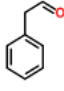
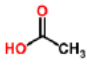
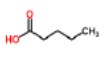
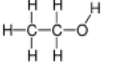
<u>Amide</u>					
Acetamide	$C_2H_5NO_2$		59	$[M+1]^+$	18
Urea	CH_4N_2O		60	$[M]^+, [M+1]^+$	18
<u>Amino acids</u>					
Ornithine	$C_5H_{12}N_2O_2$		132	$[M+1]^+$	18
Citrulline	$C_6H_{13}N_3O_3$		175	$[M+1]^+$	18
Arginine	$C_6H_{14}N_4O_2$		174	$[M+1]^+$	18
Tyrosine	$C_9H_{11}NO_3$		181	$[M+1]^+$	18
<u>Sulfonic acids</u>					
Taurine	$C_2H_7NO_3S$		125	$[M+1]^+$	18

Table SM 2. O-bearing compounds measured in the analogue laboratory experiment. Molecular weights and the defining fragment ions in the spectra are listed here.

Molecule	Formula	Struc. formula	Mol. weight	Mol. peak	defining peaks
<i><u>Ketones</u></i>					
Acetone	C ₃ H ₆ O		58	[M+1] ⁺	43
2-Butanone	C ₄ H ₈ O		72	[M+1] ⁺	43, 45 (smaller)
2-Hexanone	C ₆ H ₁₂ O		100	[M+1] ⁺	43, 45
<i><u>Aliphatic aldehydes</u></i>					
Formaldehyde	CH ₂ O		30	[M+1] ⁺	---
Propionaldehyde	C ₃ H ₆ O		58	[M+1] ⁺	43
Butanal	C ₄ H ₈ O		72	[M+1] ⁺	43, 45 (smaller)
Pentanal	C ₅ H ₁₀ O		86	[M+1] ⁺	43, 45 (smaller)
Hexanal	C ₆ H ₁₂ O		100	[M+1] ⁺	43, 45 (smaller)
<i><u>Aromatic aldehydes</u></i>					
Phenylacetaldehyde	C ₈ H ₈ O		136	---	43
<i><u>Carboxylic acids</u></i>					
Acetic acid	C ₂ H ₄ O ₂		60	[M+1] ⁺	43
Valeric acid	C ₅ H ₁₀ O ₂		102	[M+1] ⁺	43, 45 (smaller)
<i><u>Alcohols</u></i>					
Ethanol	C ₂ H ₆ O		46	[M+1] ⁺	45 (minor)

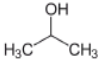


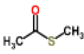
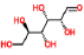
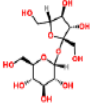
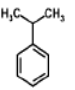
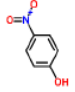
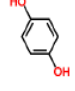
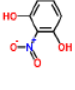
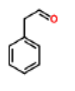
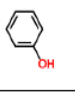
Propanol	C_3H_8O		60	$[M+1]^+$	43, 45 (minor)
Butanol	$C_4H_{10}O$		74	$[M-OH]^+$	43, 45 (smaller)
Pentanol	$C_5H_{12}O$		88	$[M-OH]^+$	43, 45 (minor)
<u>Others</u>					
S-Methyl thioacetate	C_3H_6OS		90	$[M+1]^+$	43
Glucose	$C_6H_{12}O_6$		180	---	43, 45 (smaller)
Sucrose	$C_{12}H_{22}O_{11}$		342	---	43, 45 (smaller)

Table SM 3. Aromatic compounds measured in the laboratory. Different kinds of aromatic compounds, including bicyclic and heterocyclic compounds have been measured. Aromatic fragments are observed only from mono-cyclic aromatic compounds. Here, $[M]^+$ are molecular ions. $[M+1]^+$ and $[M+2]^+$ are hydrogenated molecular ions, whereas $[M-1]^+$ are dehydrogenated ions. Aromatic fragment series is observed only from mono-cyclic aromatic compounds.

Molecule	Formula	Struc. formula	Mol. weight	Mol. peak	Aromatic fragments
<i>Aromatics: Bi-cyclic</i>					
Biphenyl-4-carboxylic acid	C ₁₃ H ₁₀ O ₂		198	---	---
Diphenylmethanol	C ₁₃ H ₁₂ O		184	$[M+1]^+$	---
1-Naphthoic acid	C ₁₁ H ₈ O ₂		172	$[M+1]^+$	---
Naphthalene	C ₁₀ H ₈		128	$[M-1]^+$	---
<i>Aromatics: N-cyclic</i>					
Nicotinic acid	C ₆ H ₅ NO ₂		123	$[M+1]^+$	---
Pyridine	C ₅ H ₅ N		79	$[M+1]^+$	---
Pyrimidine	C ₄ H ₄ N ₂		80	$[M+1]^+$	---
Quinoline	C ₉ H ₇ N		129	$[M+1]^+$, $[M+2]^+$	---
<i>Aromatics: O-cyclic</i>					
2-Furoic acid	C ₅ H ₄ O ₃		112	$[M+1]^+$	---
<i>Aromatics: I-cyclic</i>					
Aniline	C ₆ H ₇ N		93	$[M+1]^+$	77, 67, 51, 39
Benzoic acid	C ₇ H ₆ O ₂		122	$[M+1]^+$	79, 77, 67, 51
Benzyl alcohol	C ₇ H ₈ O		108	$[M+1]^+$	91, 79, 65
Benzylamine	C ₇ H ₉ N		107	$[M-1]^+$	91, 79, 65
Mandelonitrile	C ₈ H ₇ NO		133	$[M-1]^+$, M ⁺ $[M+1]^+$	79, 77, 51
p-Toluenesulfonic acid	C ₇ H ₈ O ₃ S		172	$[M+1]^+$	91, 79, 65, 53, 39
Toluene	C ₇ H ₈		92	$[M+1]^+$	---

Cumene	C_9H_{12}		120	$[M+1]^+$	---
4-Nitrophenol	$C_6H_5NO_3$		139	$[M+1]^+$	---
Hydroquinone	$C_6H_6O_2$		110	$[M+1]^+$	65
2-Nitroresorcin	$C_6H_5NO_4$		155	$[M+1]^+$	52
Phenylacetaldehyde	C_8H_8O		120	$[M+1]$	91, 77, 79, 65
Phenol	C_6H_6O		94	$[M+1]$	77, 67

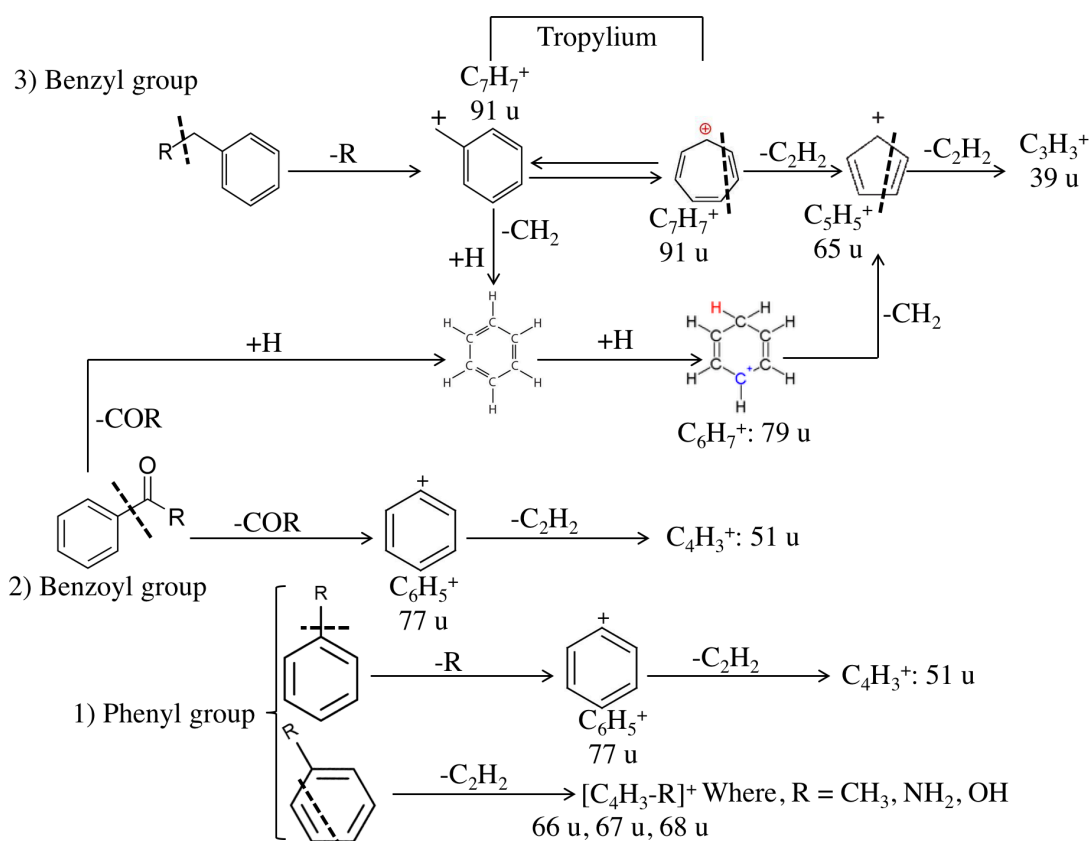


Figure SM 6. Fragmentation pathways of three groups of monocyclic aromatic compounds: Phenyl, Benzoyl and Benzyl groups (1) Phenyl group compounds lose the

attached functional group (-R) to produce a high abundance of phenyl cations at 77 u. Subsequently, phenyl cations lose acetylene ($-C_2H_2$) to produce a small peak at 51 u as $C_5H_3^+$. In another cleavage, phenyl compounds lose C_2H_2 and produce cations that reflect their functionalities i.e., $[C_5H_3-R]^+$ (2) Benzoyl group compounds also lose the attached functional group (-COR) to produce phenyl and benzenium cations at 77 u and 79 u. These also produce a small peak at 51 u due to loss of acetylene. (3) Benzyl group compounds lose functional group (-R) to form significant abundances of tropylium cations at 91 u. Subsequently, the loss of acetylene from tropylium cations produces peak at 65 u and 39 u as $C_7H_5^+$ and $C_7H_3^+$ respectively.

Table SM 4. List of 60 CDA mass spectra that have been identified as archetypal N-bearing, O-bearing-, aromatic- and mixed-types. Columns of the table are Universal time (UTC), Space Clock (SLCK), spacecraft distance to the Saturn's rotation axis in Saturnian radii (Rs), grain impact speed (V_{imp}) in km s⁻¹ and the compositional types of the ice grains. Here, "N+O", "A+N" and "A+O" refers to spectra exhibiting the mixed features of any of the two identified subtypes (N-bearing, O-bearing and aromatic), whereas "A+O+N" refers to spectra exhibiting characteristic fragments of three subtypes.

UTC	SLCK	R (Rs)	V_{imp} [km/s]	Composition (Types)
N-bearing				
2005-068/21:12:44	1489095561	7,2	8,4	N-bearing
2005-141/03:35:35	1495339372	4,0	8,3	N-bearing
2005-141/03:39:43	1495339620	4,0	8,2	N-bearing
2005-141/08:16:45	1495356242	3,9	6,4	N-bearing
2005-159/08:42:53	1496913020	3,8	8,0	N-bearing
2005-303/05:29:55	1509343122	6,1	6,7	N-bearing
2005-303/05:58:32	1509344839	6,3	6,9	N-bearing
2005-358/16:42:02	1514135479	5,4	6,1	N-bearing
2005-359/02:09:07	1514169505	5,5	6,2	N-bearing
2005-359/02:53:54	1514172192	5,7	6,4	N-bearing
2005-359/04:22:53	1514177531	6,3	6,8	N-bearing
2005-359/06:35:44	1514185502	7,2	7,2	N-bearing
2006-057/02:10:44	1519612837	9,9	6,6	N-bearing
O-bearing				
2004-302/03:15:39	1477626062	7,3	5,3	O-bearing
2004-302/03:18:43	1477626246	7,3	5,3	O-bearing
2004-302/17:50:28	1477678551	7,4	5,9	O-bearing
2004-302/17:56:59	1477678942	7,4	5,9	O-bearing

2004-302/18:21:55	1477680438	7,6	6,0	O-bearing
2004-302/21:58:20	1477693423	8,8	6,4	O-bearing
2005-068/18:41:58	1489086515	6,0	8,4	O-bearing
2005-068/21:56:39	1489098196	7,6	8,3	O-bearing
2005-302/20:59:21	1509312487	4,8	4,8	O-bearing
2005-302/21:48:16	1509315422	4,7	4,4	O-bearing
2005-302/22:17:30	1509317176	4,6	4,3	O-bearing
2005-303/04:03:16	1509337923	5,6	6,3	O-bearing
2005-303/06:15:29	1509345856	6,4	6,9	O-bearing
2005-303/07:25:44	1509350071	6,9	7,1	O-bearing
2005-358/20:16:11	1514148328	4,6	4,4	O-bearing
2005-358/21:12:29	1514151706	4,6	4,2	O-bearing
2005-359/05:24:16	1514181214	6,7	7,0	O-bearing
Aromatics				
2005-068/20:18:50	1489092327	6,8	8,4	Aromatics
2005-068/22:06:18	1489098775	7,7	8,3	Aromatics
2005-068/22:55:41	1489101738	8,1	8,2	Aromatics
2005-141/03:12:55	1495338012	4,1	8,4	Aromatics
2005-141/03:18:03	1495338320	4,1	8,4	Aromatics
2005-141/03:19:05	1495338382	4,1	8,4	Aromatics
2005-141/03:28:49	1495338966	4,0	8,3	Aromatics
2005-177/13:05:39	1498483996	4,1	8,3	Aromatics
2005-177/13:06:42	1498484059	4,0	8,3	Aromatics
2005-232/08:02:13	1503217821	4,2	8,5	Aromatics
2005-248/09:11:15	1504604371	3,5	9,3	Aromatics
2005-267/03:43:48	1506226335	5,4	9,2	Aromatics
2005-358/16:20:25	1514134182	5,6	6,3	Aromatics
2005-359/04:48:54	1514179092	6,5	6,9	Aromatics
2006-141/03:19:42	1526874621	15,5	6,3	Aromatics
2006-141/06:51:57	1526887357	14,2	6,4	Aromatics
2007-146/22:05:02	1558910345	3,7	9,9	Aromatics
2007-146/22:15:43	1558910986	3,6	9,9	Aromatics
2007-146/22:22:05	1558911368	3,6	9,9	Aromatics
2008-131/00:11:09	1589071717	4,5	14,7	Aromatics
Mixed Types				
2004-302/01:47:12	1477620755	7,7	5,7	A+N-bearing
2004-302/17:16:49	1477676532	7,3	5,8	N+O-bearing
2004-302/19:43:41	1477685344	8,0	6,2	N+O-bearing
2005-068/19:29:38	1489089375	6,4	8,4	N+O-bearing
2005-068/21:11:44	1489095501	7,2	8,4	A+N-bearing
2005-141/09:17:50	1495359907	4,3	6,9	A+N-bearing
2005-177/10:52:33	1498476010	4,9	8,6	A+O-bearing
2005-177/11:21:30	1498477747	4,7	8,6	A+O-bearing
2005-303/04:57:39	1509341186	5,9	6,6	A+O-bearing
2005-359/01:10:00	1514165958	5,2	5,7	A+O+N-bearing

2006-057/02:02:07 (1519612320)

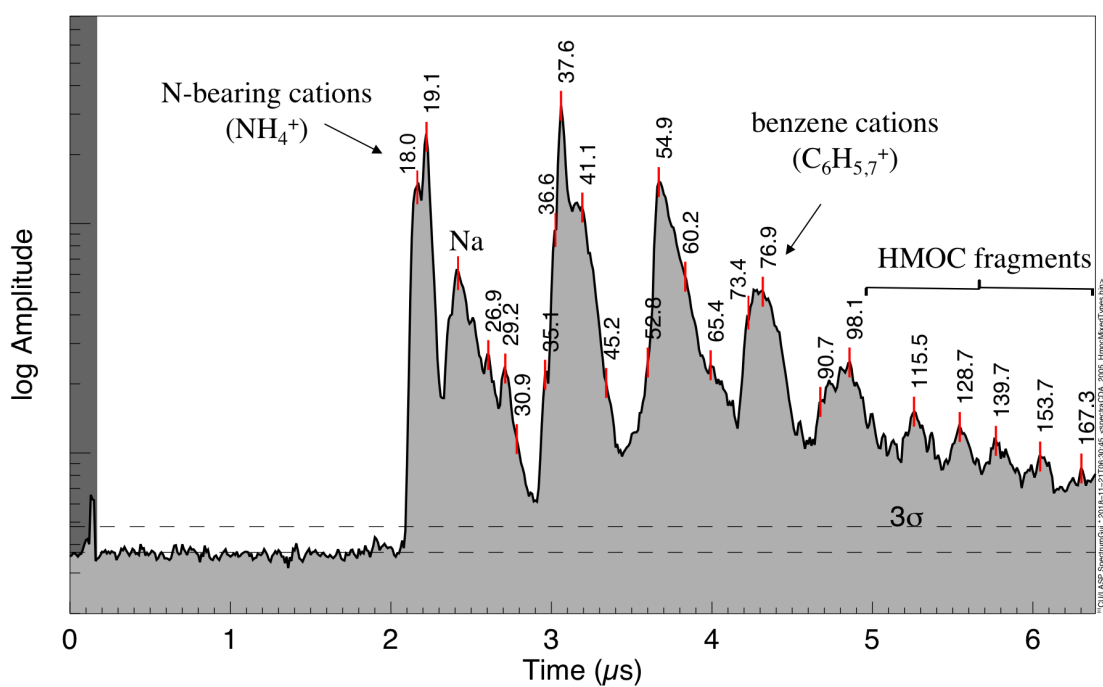


Figure SM 7. CDA Spectrum of an individual HMOC type (Postberg et al. 2018a) ice grain, containing N-bearing species, recorded at impact speeds of $\sim 6.5 \text{ km s}^{-1}$. As well as the aromatic-HMOC features mentioned in Postberg et al. (2018a), this spectrum shows diagnostic features of N-bearing compounds at 18 u from NH_4^+ . Masses are marked in unified atomic mass units.

2005-303/04:28:33 (1509339440)

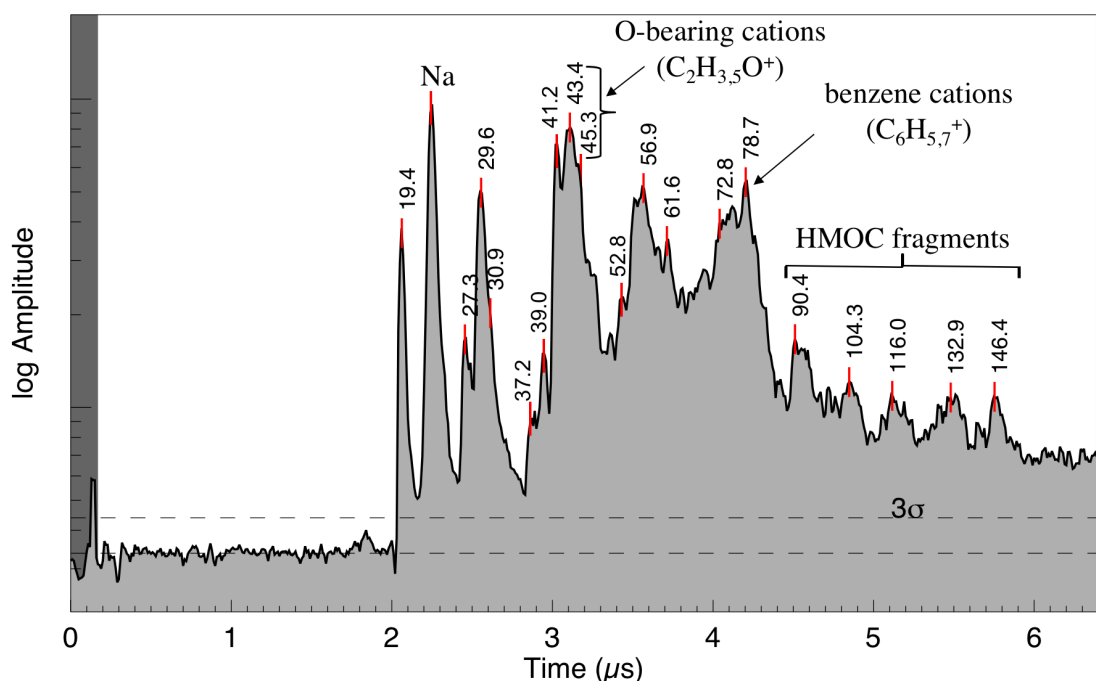


Figure SM 8. CDA Spectrum of individual HMOC type (Postberg et al. 2018a) ice grain, containing O-bearing species, recorded at impact speeds of ~ 6.5 km s $^{-1}$. As well as the aromatic-HMOC features mentioned in Postberg et al. (2018a), this spectrum shows diagnostic features of O-bearing compounds at 43 u & 45 u from C₂H_{3.5}O⁺. Masses are marked in unified atomic mass units.

Table SM 5. List of 6 CDA mass spectra that have been identified as N-bearing, O-bearing HMOC-types. These grains have already been identified as HMOC-type by Postberg et al. (2018a). Columns of the table are Universal time (UTC), Space Clock (SLCK), spacecraft distance to the Saturn's rotation axis in Saturnian radii (R), grain impact speed (V_{imp}) in km s $^{-1}$ and the compositional types of the HMOC ice grains.

UTC	SLCK	R (Rs)	V_{imp} [km/s]	HMOC (Types)
2005-068/19:57:18	1489091035	6,6	8,4	O-bearing
2005-303/04:28:33	1509339440	5,8	6,4	O-bearing
2005-303/04:48:03	1509340610	5,9	6,5	N-bearing
2005-358/14:49:12	1514128709	6,1	6,7	O-bearing
2005-359/04:06:51	1514176569	6,2	6,8	N-bearing
2006-057/02:02:07	1519612320	9,9	6,6	N-bearing

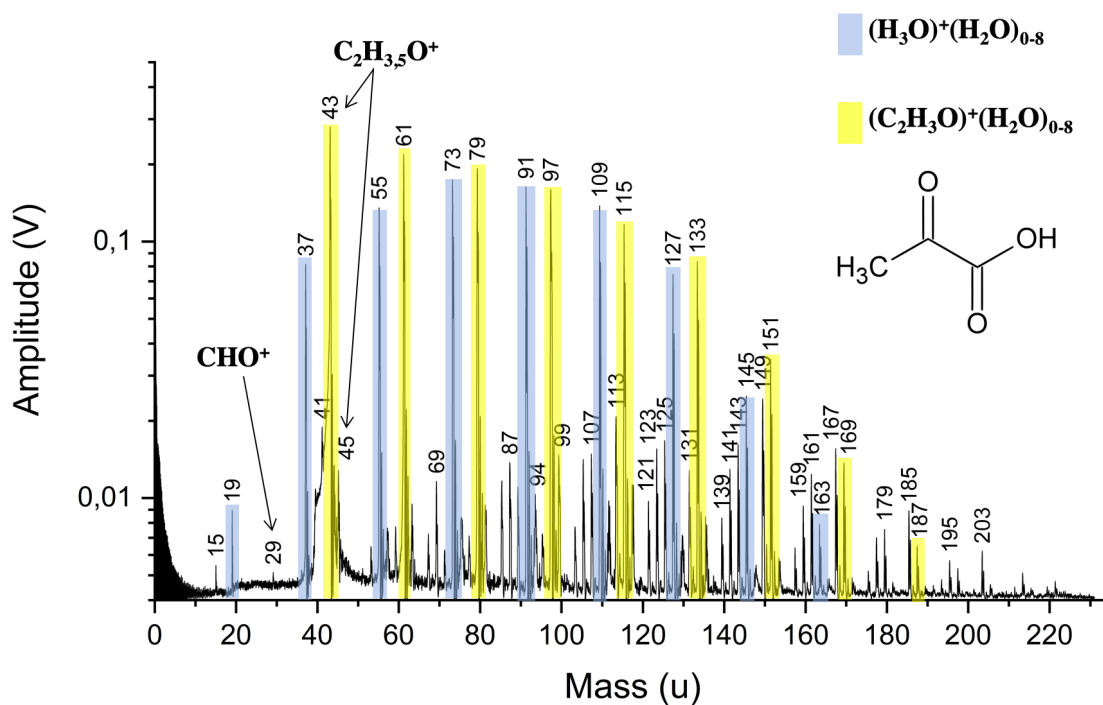


Figure SM 9: Laboratory spectrum of 0.15 molL^{-1} aqueous solution of pyruvic acid. The structure of pyruvic acid results in the fragmentation of the parent molecule to produce highly abundant acylium ions, $\text{C}_2\text{H}_3\text{O}^+$ and derivative ions at 45 u ($\text{C}_2\text{H}_5\text{O}^+$) and at 29 u (CHO^+). Blue bars show water cluster features and yellow bars represent water clusters of $\text{C}_2\text{H}_3\text{O}^+$. The abundant formation of water cluster from acylium ions as well as the suppressed low amplitude of H_3O^+ at 19 u are in agreement with most of the O-bearing CDA spectra.

D)

In this section, we present an application of our results, together with those from Bouquet et al. (2019), Szentirmai et al. (2016) and Wakelam et al. (2017), to the INMS Enceladus plume species from Magee & Waite (2017). Spectral appearance, binding energies and vapour pressure are used to discount the transfer of species to the ice grains from the gas phase.

Although few published values for the binding energies with crystalline water ice of the species identified by INMS (Magee & Waite 2017, Postberg et al. 2018b) are available, calculated values of many of the compounds with amorphous ice are (Wakelam et al. 2017). A comparison of values for crystalline and amorphous ice, using overlapping data from Bouquet et al. (2019) and Wakelam et al. (2017), indicates that, with the exception of Formaldehyde - which is noted to have unusual behaviour (Bouquet et al. 2019), the more polar substances tend to have higher binding energies with crystalline water ice than amorphous, whereas the less polar (e.g. hydrocarbons) have higher binding energies with amorphous ice than crystalline. Based on the behaviour of ethanol and methanol, we estimate that a lower limit to the binding energy with amorphous ice of 0.42 eV will result in residence times similar to those found for species with binding energies of 0.5 eV with crystalline ice, given in Bouquet et al., 2019, and use this where necessary in Table 2.

Table SM 6 shows the results of applying spectral appearance, binding energy and vapour pressure constraints to the species detected by INMS in Enceladus' plume. The detailed criteria are described in the main text. Based on these results compounds are assigned varying levels of likelihood as to their ability to enter the gas phase and subsequently adsorb onto icy surfaces as shown in Table 2.

Table SM 6: Adapted from Magee & Waite (2017) the table shows whether organic species detected in the plume fulfil criteria (binding energy and vapour pressure) indicative of their ability to enter E ring grains and produce spectral features in agreement with Type 2N and 2O spectra. Here, “Y” means “possible”; “X” means not possible and “Z” means no information is available. We do not exclude species assigned “Z”. Organic species with multiple isomers are also given where possible. For hydrocarbons, generic names are used.

Organic class	Formula	Species (isomers)	Mol. structure	Binding energy (eV)	Vapour pressure (kPa)
N-bearing	HCN (27)	hydrogen cyanide	X	X	Z
	N ₂ (28)	nitrogen	X	X	Z
	CH ₅ N (31)	methylamine	Y	Y	Y
	C ₂ H ₃ N (41)	acetonitrile/azirine	X/X	X/Z	Z/Z
	C ₂ H ₇ N (45)	ethyl amine/dimethyl amine	Y/Y	Z/Z	Y/Y
	C ₂ H ₆ N ₂ (58)	azomethane/methylammonium cyanide	X/Y	Z/Z	Y/Y
	C ₄ H ₉ N (71)	pyrrolidine	X	Z	Z
	C ₄ H ₈ N ₂ (84)	4- & 2- amino butane nitrile / 3- methylamino propionitrile	Y&Y/Y	Z&Z/Z	Z&Z/Z
	C ₆ H ₁₂ N ₄ (140)	methenamine	X	Z	Z
	O-bearing	CO (28)	carbon monoxide	X	X
CH ₂ O (30)		formaldehyde	X	X	Y
O ₂ (32)		oxygen	X	X	Z
CH ₃ OH (32)		methanol	X	Y	Y
C ₂ H ₂ O (42)		ethenone/ethynol	Y/X	X/Z	Y/Z
C ₂ H ₄ O (44)		acetaldehyde/ethylene oxide	Y/Y	Y/Z	Y/Y
C ₂ H ₆ O (46)		ethanol/dimethyl ether	X/X	Y/Z	Y/Y
C ₃ H ₆ O (58)		acetone/propanal/allyl alcohol/methyl vinyl ether/propylene oxide	Y/Y/X/Y	X/Z/Z/Z	Y/Y/Y/Z/Y
C ₃ H ₈ O (60)		1- & 2- propanol/ethyl methyl ether	Y/Y/Y	Y&Z/Z	X&X/Y
C ₂ H ₄ O ₂ (60)		acetic acid / methyl formate	Y/Y	Y/Z	Y/Z
C ₂ H ₆ O ₂ (62)	ethylene glycol	Y	Z	Z	
C ₄ H ₁₀ O (74)	1- & 2- butanol/isopropyl methyl ether	Y&Y/Y	Y&Z/Z	X&Y/Y	
C ₄ H ₆ O ₂ (86)	vinyl acetate/2-butyne-1,4-diol/2,3-butanedione/2-butenic acid	Y/X/Y/Y	Z/Z/Z/Z	Z/Z/Y/Z	
NO-bearing	NO (30)	nitric oxide	X	X	Z
	C ₂ H ₇ NO (61)	ethanolamine/ N, O-dimethylhydroxyl amine/ N, N-dimethylhydroxyl amine	Y/Z/Z	Z/Z/Z	Z/Y/Z
	C ₂ H ₅ NO ₂ (75)	glycine/ methyl carbamate/ethyl nitrite/nitroethane	Y/Y/Y/X	Z/Z/Z/Z	Z/Z/Y/Z
	C ₃ H ₇ NO ₂ (89)	alanine / 1- & 2- nitropropane / isopropyl nitrite	Y/Y&Y/Y	Z/Z&Z/Z	Z/Z&Z/Y
Hydrocarbons	C ₂ H ₂ (26)	acetylene	X	X	Y
	C ₂ H ₄ (28)	ethylene	X	X	Y
	C ₂ H ₆ (30)	ethane	X	X	Y
	C ₃ H ₄ (40)	propyne	X	X	Y
	C ₃ H ₆ (42)	Propene	X	X	Y
	C ₃ H ₈ (44)	propane	X	X	Y
	C ₄ H ₈ (56)	butene	X	Z	Y
	C ₄ H ₁₀ (58)	butane	Y	Z	Y
	C ₅ H ₁₀ (70)	pentene	X	Z	Y
	C ₅ H ₁₂ (72)	pentane	Y	Z	Y
C ₈ H ₁₈ (114)	octane	Y	Z	Y	
Others	C ₃ H ₅ Cl (76)	allyl chloride / 1-&2-chloropropylene	X/X&X	Z/Z&Z	Y/Y&Y

REFERENCES

- Bouquet A., Glein C. R., Waite J. H., 2019, *The Astrophysical Journal*, 873 (1), 13.
- Charvat A., Lugovoj E., Faubel M., Abel B., 2004, *Review of Scientific Instruments*, 75(5 PART 1), 1209–1218.
- He J., Acharyya K., Vidali G., 2016, *The Astrophysical Journal*, 825:89.
- Hillier J. K. et al., 2007, *MNRAS*, 377(4), p. 1588–1596.
- Klenner F. et al., 2019, *Rapid Communications in Mass Spectrometry*, doi:10.1002/rcm.8518.
- Le Roy L., Bardyn A., Boris C., Cottin H., Fray N., Thirkell L., Hilchenbach M. 2015, *Planetary and Space Science*, 105, pp 1-25.
- McLafferty F. W., Turecek F., 1993, *Interpretation of mass spectra*, University Science Books, California, Vol. 04.
- Postberg F., Kempf S., Srama R., Green S. F., Hillier J. K., McBride N., Grün E., 2006, *Icarus*, 183, 122–134.
- Postberg F., Kempf S., Hillier J. K., Srama R., Green S. F., McBride N., Grün, E., 2008, *Icarus*, 193, 438–454.
- Postberg F., Kempf S., Schmidt J., Brilliantov N., Beinsen A., Abel B., Buck U., Srama R., 2009a, *Nature*, 459, 1098–1101.
- Postberg F., Kempf S., Rost D., Stephan T., Srama R., Trieloff M., Mocker A., Goerlich M., 2009b, *Planet. Space Sci.* 57, 1359–1374.
- Postberg F., Schmidt J., Hillier J., Kempf S., Srama R., 2011, *Nature* 474, 620–622.
- Postberg F. et al., 2018a, *Nature*, 558, 564–568.
- Srama R. et al., 2004, *Space Science Reviews*, 114(1–4), 465–518.
- Srama R. et al., 2009, *Rapid Comm. Mass Spec.* 23, 3895–3906.
- Szentermai V., Szori M., Picaud S., Jedlovszky P., 2016, *JPC*, 120, p. 23480-23489.
- Wiederschein F. et al., 2015, *PCCP*, 17(10), 6858–64.
- Wakelam V., Loison, J.-C., Mereau, R., Ruaud, M. 2017, *Molecular Astrophysics*, 6, p. 22-35.